Bulletin of the Seismological Society of America, Vol. 106, No. 5, pp. 2332–2344, October 2016, doi: 10.1785/0120160010

Implementing the ElarmS Earthquake Early Warning Algorithm on the Israeli Seismic Network

by Ran N. Nof and Richard M. Allen

Abstract Earthquake early warning systems (EEWS) are being operated and tested increasingly around the globe in recent years. Following the Israeli government's decision to build an EEWS in Israel, and as the Californian EEWS (ShakeAlert) moves toward its operational phase, we demonstrate implementation of one of its three algorithms, ElarmS, to the Israel region. We provide new tools and approaches for implementing and assessing ElarmS outside of California. The main challenges of this research are to identify, verify, and adjust the embedded location-dependent parameters in ElarmS to the Israeli region, utilizing an unoptimized seismic network and low seismicity rate. To this end, we run ElarmS in three different modes: (1) historical playbacks, (2) real-time continuous data processing, and (3) simulated data playbacks. These modes enable us to overcome the limitations of low seismicity rates in the region and evaluate the performance of ElarmS with the network that is currently available. We use historical playbacks to adjust the magnitude estimation equations of ElarmS. We then analyze real-time processing results and provide detailed analysis of two significant events in the region (M_D 5.5 and 4.4). Finally, we provide the first case of how to use synthetic data to evaluate the performance of ElarmS. We find that alert times are mostly affected by the network geometry and also by data delays. Alerts are typically issued within 80 ms after the arrival of the required four P-wave triggers data to the system. Magnitude estimations are reliable for events with $M_D > 3.5$ within 100 km of the Israeli network using a locally adjusted magnitude relation equation.

Introduction

Earthquake early warning systems (EEWS) are being adopted around the globe and are currently operating in Mexico (Espinosa-Aranda *et al.*, 2011), Japan (Nakamura, 1988), Taiwan (Hsiao *et al.*, 2009), Romania (Ionescu *et al.*, 2007), California (Kuyuk, Allen, *et al.*, 2014), and being tested in Italy (Satriano *et al.*, 2011), South Korea (Sheen *et al.*, 2014), Turkey (Erdik *et al.*, 2003), and other places. Several algorithms for EEW exist, such as ElarmS (Kuyuk, Allen, *et al.*, 2014), PRESTo (Satriano *et al.*, 2011), Virtual Seismologist (Cua *et al.*, 2009), OnSite (Böse *et al.*, 2009), and UrEDAS (Nakamura and Saita, 2007). The basic concept of EEW is to detect and estimate earthquake parameters, such as location, magnitude, and origin time, in the shortest amount of time possible and to deliver an alert to populated areas before the arrival of more destructive waves. This goal is achieved by processing instrumental measurements of velocity or acceleration from one (e.g., OnSite) or more (e.g., ElarmS) stations and estimating magnitudes based on proxies such as the maximal amplitude or the frequency content of the first few seconds after the arrival of the P or S wave.

In California, three algorithms are being tested under the California Integrated Seismic Network (CISN) ShakeAlert system, with an aim to demonstrate the feasibility of EEW in California. The ShakeAlert decision module (DM) combines the event estimations from all three algorithms implemented in parallel (OnSite, Virtual Seismologist, and ElarmS) and reports the most probable earthquake magnitude and location to a group of test users from private industry and emergency response organizations in California (Böse *et al.*, 2014). The ElarmS algorithm is maintained at the University of California Berkeley Seismological Laboratory and is under constant evaluation and development.

Recently, ElarmS successfully provided an alert for the 24 August 2014 South Napa M_w 6.0 event. Performance evaluations for 2014 show that ElarmS sent out successful alerts for all significant earthquakes and aftershocks within the California border ($M_w \geq 4.5$, 10 earthquakes), with no false alerts and within 0.5 magnitude units of the catalog magnitudes. The alert time for the Napa mainshock was 5.1 s after the earthquake origin time and was dependent on the density of the seismic network around the epicenter (Kuyuk and Allen, 2013b; Allen *et al.*, 2015). Within the ShakeAlert system, ElarmS frequently provides the most rapid alerts and rarely issues false alerts.

ElarmS is highly customized to California and its various real-time (RT) networks. This localized customization includes many parameterizations and models, such as the relationships of the main magnitude proxies (maximum displacement P_d and dominant period T_P; Allen *et al.*, 2009); the fixed event depth of 8 km; a velocity model for the California region; and other factors. Implementing ElarmS algorithms in a different region is expected to require some adjustments to the user-defined, or the hard-coded, parameters (Sheen *et al.*, 2014). In this work, we lay out the implementation of ElarmS EEWS algorithms to the Israeli Seismic Network (ISN) as the first example of the algorithm's RT performance outside of California.

Israel is located adjacent to the Dead Sea Transform (DST), a tectonically active plate-boundary fault system (e.g., Garfunkel *et al.*, 1981). The DST and its branches, the Yamouneh, Roum, and Carmel faults (Fig. 1), are capable of producing earthquakes with maximum magnitudes of M_w 7.5–7.8 (Yucemen, 1992; Shapira and Hofstetter, 2007; Hamiel *et al.*, 2009; Levi *et al.*, 2010). Based on paleoseismic, historic, and instrumental records, recurrence times are on the order of 100 and 1000 yrs for M_w 6 and 7 earthquakes, respectively (Shapira and Hofstetter, 2007; Levi *et al.*, 2010). The most recent destructive earthquake along the DST was the 1927 M_L 6.2 earthquake near Jericho (Shapira *et al.*, 1993), which led to 285 deaths and ~1000 injured in the area (Avni *et al.*, 2002). Given the growth in population during the past century and the expected recurrence interval of destructive earthquakes, the increased seismic risk for Israel has led the Israeli government to instruct the Geological Survey of Israel to establish an EEWS for Israel. Following recommendations of an international committee (Allen *et al.*, 2012), the proposed system would include an upgrade to the current ISN; which translates into adding ~100 new stations of strong-motion accelerometers and broadband velocity instruments along the major fault line of the DST and its Carmel fault branch (Pinsky, 2015). The collected data would be processed by an EEW algorithm in order to deliver rapid alerts for potentially damaging earthquakes.

The main challenge of our current research is to identify, verify, and adjust the embedded location-dependent parameters in ElarmS to Israel and the broader DST region. These goals are achieved by running the ElarmS system using data from the ISN in different modes: (1) historical playbacks: processing archived data and historic records collected at the Geophysical Institute of Israel (GII), playbacks can be run at an RT speed (real-time playback [RTP]) or at an accelerated speed (accelerated-time playback [ATP]); (2) RT data: processing the current ISN data streaming to the GII continuously; and (3) simulation playback: processing simulated event data playbacks for various earthquake scenarios.

Playback capability was only recently implemented for ElarmS, and was initially limited to preprocessed results

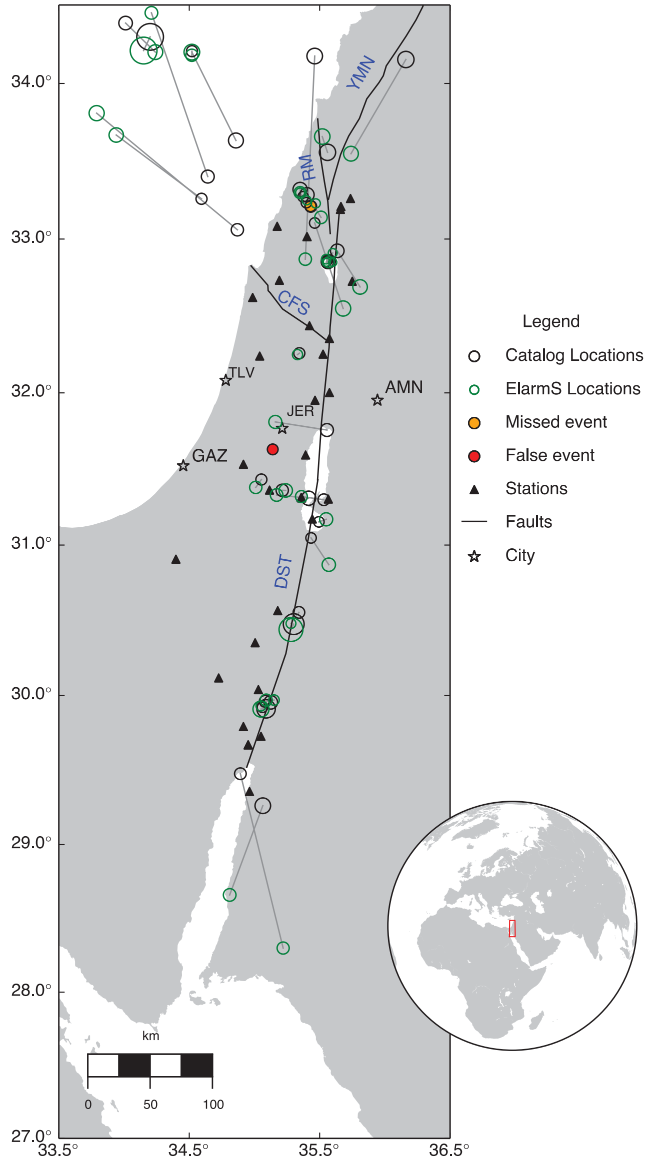

Figure 1. Events locations calculated by ElarmS. First reported locations of "Matched" events are presented as green circles scaled by estimated magnitude. Gray lines point to the Geophysical Institute of Israel (GII) catalog location marked as black circles. Missed events are marked as orange circles and False events as red circles. Stations used for playback are marked by triangles. Generalized major fault systems are marked as black lines: DST, Dead Sea Transform; CFS, Carmel fault system; YMN, Yamouneh fault; and RM, Roum fault. Major cities are marked by white stars: JER, Jerusalem; AMN, Amman; TLV, Tel-Aviv; and GAZ, Gaza. The inset shows the global location of the map in the red rectangle.

collected in RT (Kuyuk, Allen, *et al.*, 2014), which meant that playback capability could not be used efficiently for new data. To this end, a set of tools were created to analyze ElarmS results in RT and in playbacks (i.e., RTP or ATP), using archived or simulated data (see Appendix). Below, we present the results of our analysis of historical data playback processing for 39 events with coda magnitudes (Shapira, 1988) $M_D > 3$, between January 2012 and May 2015, followed by an analysis of different aspects of RT processing and performance, including detailed system performance for two $M_D > 4$ events. We then provide a summary of simulated data playback processing of four earthquake scenarios. Finally, the implications of implementing ElarmS outside of California, and more specifically to the Israeli region, are presented in light of these results.

Historical Data Playbacks

The high seismicity rate in California provides ample RT data to regularly evaluate ElarmS performance. However, in Israel, the lower seismicity rate in the region along the DST (based on 60,000 yrs of prehistoric-paleoseismic, historic, and instrumental records) indicates lower recurrence intervals of 5 and 15 yrs for $M_w \geq 4.5$ and $M_w \geq 5.0$ earthquakes, respectively (Hamiel *et al.*, 2009). Thus, it is essential to use historical data to evaluate ElarmS near the DST, in addition to analyzing the RT performance of the system in Israel with smaller magnitude earthquakes.

The ability to run historical data in RTP is available within the native ElarmS. However, running multiple events spanning several minutes is a time-consuming task. Therefore, an ATP capability was introduced into the ElarmS code for this research, allowing the algorithm to run in simulated RT. This method of playback enables us to run historical data in ~30% of RT (~3 times faster than RT) depending on the amount of data (i.e., number of traces, sampling rate) and server speed. For example, by using five simultaneous processors, 21 min of 239 traces (23 MB) are processed in 412 s (~30% of RT). Moreover, processing time can be further reduced if data are provided in packets (typically of 1 s) ordered by packet starting time. This process of packetization reduces the processing time for the above example to 120 s (~10% of RT). Therefore, a whole day's worth of prepacked RT data might be completed in ~2.5 hrs.

We note that playbacks can only be used to compare ElarmS performance under different scenarios (including parameter settings) and should not be used as a method of reproducing the exact chain of processing as it would play out in RT.

Playback Data and Processing

We processed data from 39 events ($M_D > 3.0$) in the GII catalog in ATP mode (Table 1). The dataset includes all of the events categorized as earthquakes by GII analysts, occurring from February 2012 to May 2015 within the geographical boundaries of 29.0°–34.5° latitude and 33.0°–37.0° longitude (see Fig. 1 for event locations).

ElarmS only issues an alert if four or more stations are triggered, and only when those alerted stations represent more than 40% of the active stations located within the epicentral distance radius to the farthest triggered station. In addition, several threshold tests are performed to prevent alerting on teleseismic or low magnitude ($M_w < 2$) events (Kuyuk, Allen, *et al.*, 2014). We use the default settings of ElarmS, as used in the ShakeAlert system, and provide both a channel list and a set of parameters corresponding to the ISN. In addition to data archived from 23 broadband (BB) and short-period ISN core stations, we use available data from neighboring networks including five BB stations from the Jordanian Seismic Network (JSN) and seven BB stations from the Geophone Network (GE) located along the DST, Cyprus, and Turkey, all of which are archived at the GII. Data were additionally reorganized into 1 s packets. ElarmS continuously re-estimates event solutions (i.e., origin time, location, and magnitude) as new data arrive, potentially improving the solution accuracy. In our analysis though, only the first alert is evaluated because the initial alert is expected to have the most impact on the earthquake mitigation actions taken. We quantitatively estimate the ElarmS Performance Score (PS) as the ratio between real detected and alerted events (true) and the sum of True, undetected real events (missed), and false alerted events (false):

$$\mathrm{PS} = \frac{T}{T + M + F} \times 100, \qquad (1)$$

in which T, M, and F are the true, missed, and false events, respectively.

Playbacks Results

Of the 39 events that we looked at, ElarmS produced triggers and issued alerts for 38 of these events. The remaining event was also detected, but no alert was issued because it failed the teleseismic test (Kuyuk, Allen, *et al.*, 2014), which marked it as a distant event. In addition, one false event was generated and ElarmS issued an alert due to the problem of associating distant ($R > 300$ km) station triggers with a true event. The PS for the 39 historical events is 95.0%. However, data tested here include packets from only 10 min before to 10 min after each event so false alert susceptibility was not fully tested.

We distinguish between station magnitudes (estimated at each individual station) and event magnitudes (calculated for an event solution based on the average of the contributing station magnitudes). ElarmS station magnitudes (M_w) are estimated separately at each station that were triggered, based on the maximum displacement (P_d) with the relation (Kuyuk and Allen, 2013a):

$$M_w = 5.39 + 1.23 \log_{10}(P_d) + 1.38 \log_{10}(R), \qquad (2)$$

in which P_d is in centimeters and R is the epicentral distance in kilometers. This relation was calculated using offline data from three regions: northern and southern California archives, Japan, and RT results from California, resulting in a 0.01 average magnitude error and 0.31 standard deviation (st. dev.) in magnitude errors (Kuyuk and Allen, 2013a). The event magnitude is calculated as the average of the station magnitudes, omitting stations with low signal-to-noise ratio

Table 1
List of Geophysical Institute of Israel (GII) Catalog Events Used for Playbacks

Event ID	M_D	Latitude (°)	Longitude (°)	Date (yyyy/mm/dd)	Time (hh:mm:ss.sss)	ElarmS Detection*
201202091110	3.10	32.856	35.553	2012/02/09	11:11:56.360	Alerted
201203070846	3.68	33.286	35.403	2012/03/07	08:47:52.914	Alerted
201203071404*	3.25	33.213	35.430	2012/03/07	14:06:12.330	Missed (teleseismic)
201203080114	3.26	33.211	35.432	2012/03/08	01:15:53.226	Alerted
201203220415	3.74	31.309	35.415	2012/03/22	04:17:03.772	Alerted
201203241159	3.20	33.260	34.594	2012/03/24	12:01:08.397	Alerted
201205111847	5.30	34.297	34.200	2012/05/11	18:48:30.461	Alerted
201207101733	3.70	33.320	35.350	2012/07/10	17:34:59.527	Alerted
201207211701	3.11	33.273	35.373	2012/07/21	17:02:59.833	Alerted
201208110359	3.60	29.955	35.125	2012/08/11	04:00:47.268	Alerted
201208151538	3.30	29.962	35.082	2012/08/15	15:39:18.339	Alerted
201210081913	3.90	29.262	35.064	2012/10/08	19:14:38.505	Alerted
201211031956	3.40	33.060	34.869	2012/11/03	19:57:15.75	Alerted
201211180352	3.10	33.104	35.462	2012/11/18	03:54:04.330	Alerted
201211180919	3.10	31.153	35.494	2012/11/18	09:19:52.458	Alerted
201212241443	4.30	29.912	35.089	2012/12/24	14:44:39.810	Alerted
201306010842	3.10	31.047	35.434	2013/06/01	08:43:46.509	Alerted
201306112121	3.30	30.554	35.341	2013/06/11	21:22:14.49	Alerted
201308080824	3.20	34.206	34.521	2013/08/08	08:25:41.152	Alerted + false event
201309120118	3.50	31.757	35.556	2013/09/12	01:20:03.357	Alerted
201310171816	3.50	32.851	35.565	2013/10/17	18:17:53.361	Alerted
201310200848	3.60	32.854	35.564	2013/10/20	08:50:03.486	Alerted
201310201252	3.50	32.857	35.571	2013/10/20	12:54:05.803	Alerted
201310220539	3.30	32.847	35.559	2013/10/22	05:40:49.884	Alerted
201310231232	3.30	29.477	34.892	2013/10/23	12:33:53.308	Alerted
201312071121	3.20	31.432	35.053	2013/12/07	11:22:45.261	Alerted
201312122101	3.40	31.361	35.213	2013/12/12	21:02:22.969	Alerted
201401131300	3.60	32.924	35.635	2014/01/13	13:01:45.45	Alerted
201402240050	3.10	33.235	35.398	2014/02/24	00:52:13.783	Alerted
201402281922	3.20	32.259	35.344	2014/02/28	19:24:01.102	Alerted
201403230455	3.60	34.385	34.012	2014/03/23	04:55:43.888	Alerted
201405240726	4.60	30.476	35.301	2014/05/24	07:27:30.657	Alerted
201405251221	3.90	34.175	35.462	2014/05/25	12:22:54.440	Alerted
201406140717	3.10	29.922	35.061	2014/06/14	07:18:21.111	Alerted
201407021004	3.50	33.403	34.642	2014/07/02	10:05:46.883	Alerted
201407052140	4.00	33.559	35.560	2014/07/05	21:41:34.222	Alerted
201409012049	4.00	34.153	36.161	2014/09/01	20:50:08.43	Alerted
201501061701	3.30	31.299	35.532	2015/01/06	17:02:30.964	Alerted
201502141148	3.80	33.635	34.858	2015/02/14	11:50:07.385	Alerted

*ElarmS detection column indicates the true (alerted), missed, and false events.

(SNR) or stations with epicentral distances greater than 100 km, provided that closer stations are available.

Magnitude estimates for events in Israel from ElarmS in ATP mode show underestimation for most of the events (Fig. 2, top). The misfit of event magnitude estimations is in the range of −1.8 to 0, with a mean underestimation of 0.88 magnitude units and a standard deviation of 0.46 (Fig. 3a). Similarly, the station magnitude estimates used for event magnitude calculations (total of 154) show a mean magnitude error of −0.91 with st. dev. of 0.78 (Fig. 3a). The median location error is 8.7 km, whereas 24% exceed 50 km (Fig. 3c) and the median absolute origin-time error is 1.5 s, with 24% of the solutions exceeding 5 s (Fig. 3d). The larger location and origin-time errors correspond to the distance between the epicenter and the ISN stations (Fig. 1), where events located further away from the network are more prone to large errors. This is expected as the system is suited to in-network events, whereas it performs less well for out-of-network events.

The station magnitude calculation, equation (2), takes into account the epicentral distance to the event, hence, a location error can propagate into a magnitude error. In an attempt to probe the origin of the magnitude errors, we confirm that the magnitude offsets cannot be simply correlated with location errors, origin-time errors, or with SNR.

Instead, we examine a locally derived magnitude to P_d relation using a set of 95 historical earthquakes between $2.5 \leq M_D \leq 5.3$ recorded by the GII between 2002 and 2011. Sadeh *et al.* (2014) found a regional magnitude to P_d^* relation for Israel:

$$\log_{10}\left(P_d^* \times \frac{R}{R_{\text{ref}}}\right) = 1.041 M_D - 10.031, \quad (3)$$

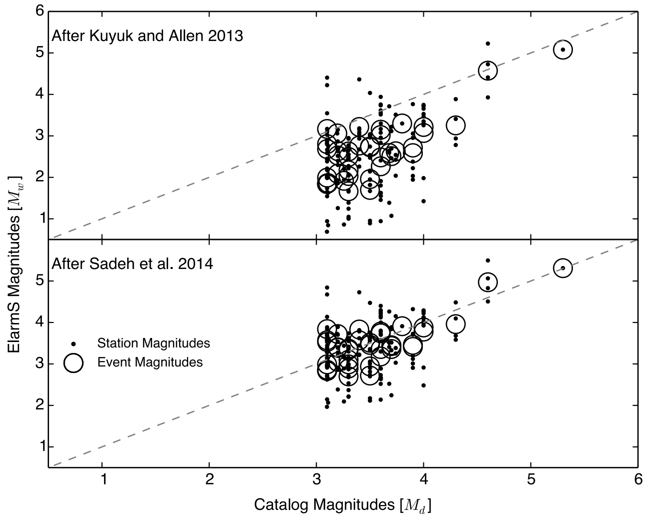

Figure 2. Playback magnitudes. ElarmS versus GII catalog magnitudes. Event magnitudes are marked as open circles, stations magnitudes used for calculating the events magnitudes are marked as dots. (Top) Using P_d–magnitude relations after Kuyuk and Allen (2013a) and (bottom) using P_d–magnitude relations after Sadeh *et al.* (2014).

in which P_d^* is in meters, R is the epicentral distance in kilometers, and R_{ref} is an arbitrary reference distance set at 100 km. Equation (3) can be rewritten in the form of equation (2) as

$$M_D = 5.7935 + 0.96061(\log_{10} P_d + \log_{10} R), \quad (4)$$

in which P_d is now in centimeters.

We recalculated the event and station magnitudes using equation (4), which yielded a significant improvement and subsequently eliminated the magnitude offsets (Fig. 2, bottom), with an event mean magnitude error of 0.08 and st. dev. of 0.34 (similar to the calculated st. dev. by Kuyuk and Allen, 2013a, for a more global dataset). Station magnitudes errors were further reduced to a mean value of −0.08 and a 0.6 st. dev. after recalculation (Fig. 3b). Finally, we implemented the new scaling equation to ElarmS and verified that we obtained the same results in a rerun of the playbacks.

The disparity of the coefficients of the scaling equations (2) and (4) might be explained by the differences in the geologic structures of the Israel region and the California/Japanese regions that were used to derive the two empirical relations. Similar differences leading to an underestimation of peak ground acceleration have also been shown by Campbell and Bozorgnia (2006), who compared ground-motion prediction equations (GMPEs) derived from global data and GMPEs, which were devised for Europe and the Middle East by Ambraseys *et al.* (2005). Hereafter, we use the local magnitude scaling relation of Sadeh *et al.* (2014) instead of the global relations derived by Kuyuk and Allen (2013a).

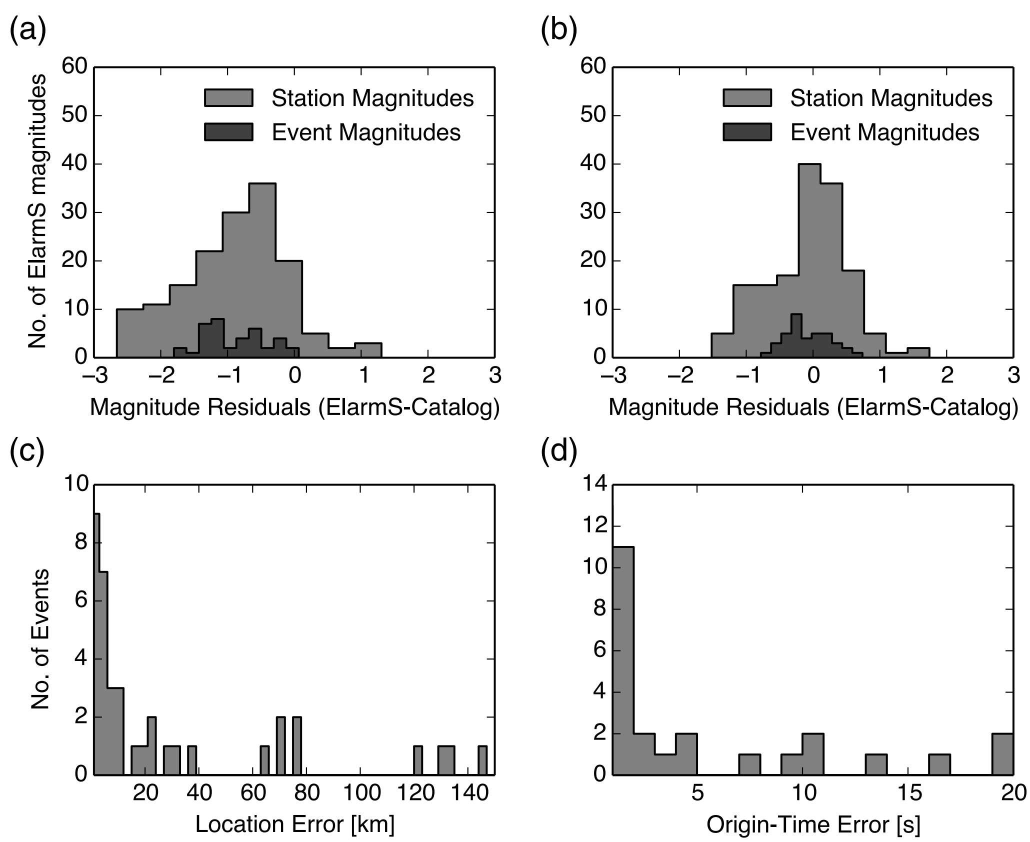

Figure 3. Histograms of errors for historical playback data: (a) magnitudes errors using Kuyuk and Allen (2013a) scaling, (b) magnitudes errors using Sadeh *et al.* (2014) scaling, (c) locations errors, and (d) origin-time errors.

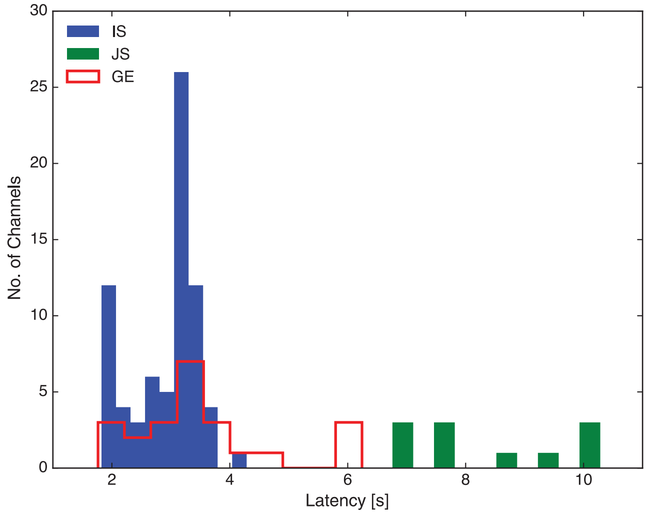

Figure 4. Latencies histogram for the Israeli seismic network stations (IS, blue), the Royal Jordanian Seismic Observatory stations (JS, green), and the Geophone Network stations (GE, red) used by the GII.

The missed event, flagged as teleseismic by ElarmS, is not actually a teleseismic event. Indeed, the event average P_d and T_P values did not meet the threshold needed to be considered a local event by ElarmS (see equation 2 in Kuyuk, Allen, *et al.*, 2014), but they were very close to this threshold. The simple linear threshold used to differentiate teleseismic events from local events might need further adjustments for the Israeli region.

The false alert was based on triggers that should have been associated with event 201308080824 (Table 1). ElarmS associates new triggers to an event if the measured travel time falls within a certain time window, defined by a calculated *P*-wave travel time plus or minus a few seconds. This misassociation suggests that the time-window calculation should be adjusted to the local velocity structure.

Real-Time Performance

ElarmS has been running at the GII on a testing server since November 2014. For our current work, we modified the ElarmS code to (a) enable RTP and ATP, (b) to produce more detailed and coherent log files suitable for analysis, (c) to fix some minor bugs, and (d) to adjust for the new geographical location. Because of these changes and because of the inconsistency of older log files, RT results are only available since May 2015. Further analysis of the RT performance will be examined in the future. Data analysis presented here is from 1 May to 31 July 2015.

ISN Latencies and Delays

Latency is defined here as the difference between the time-stamp for the final measurement sample in a waveform packet and the arrival time of the same packet at the ElarmS data buffer. This includes the time needed for the data logger to pack the measurements and send the packet, plus the travel time of the packet, through a telemetry system (e.g., radio, internet, satellite, etc.). Delays are defined here as the difference between the time-stamp of a sample within the packet and the arrival time of that same sample to the buffer. Delays encompass the time between the sample of interest and the end of the data packet, plus the latency. For the ShakeAlert system in California, the latency for most of the networks is less than 2 s (less than 1 s for most of Berkeley [BK] and southern California [CI] stations) and most of the packet sizes are 1 s.

GII station latencies were measured over several hours on 1 May 2015. Though the ISN is not optimized for rapid RT acquisition, latencies for data arrivals are mostly below 4 s (mean latency 2.9 s). Additional stations, acquired from JSN and GE, have longer mean latencies of 8.4 s and 3.5 s, respectively (Fig. 4). However, despite the reasonable latencies, waveform packet sizes span 1–9 s (6 s on average) for the ISN stations. These long packets will delay trigger detection by half the packet length on average. For example, if the trigger is within the first samples of a 9 s packet, this would lead to a potential alert delay of ~10 s compared with the alert time for a 1 s packet waveform. This is because the full packet needs to be created and sent before the trigger is identified by the ElarmS triggering module.

Real-Time Results

During the course of our analysis period (1 May 1 to 31 July 2015), 76 alerts were issued by ElarmS (events magnitude threshold is $M_w > 3.0$). The GII catalog contains seven events of $M_w > 3.0$ for this period with locations between 33.5° to 36.5° longitude and 28.7° to 34.7° latitude. Comparing the ElarmS alerts with the catalog, based on the space–time proximity of the ElarmS and catalog locations and origin time, matched 75 events (including overestimated catalog events of $M_D < 3.0$), 2 missed events and 1 false event. The missed events were M_D 3.5 and 4.3 events in the Mediterranean Sea ($R > 140$ km) and the ElarmS teleseismic test suppressed these alerts. The false event (M_w 3.4) was a result of misassociation of triggers from an M_w 4.9 event in south Turkey ($R > 400$ km) similar to what we observed previously in the playback false alert. We found that ElarmS issued alerts based on an overestimation of 70 events (Fig. 5).

The GII analysis team categorized nearly all of the events for which ElarmS overestimated the magnitudes as explosions (67 out of 70 events), based on the frequency content of the *P* and *S* waves, their location and other considerations. The overestimation of magnitudes of quarry blasts could be a consequence of the different physical mechanisms behind explosions and natural earthquakes. Larger *P*-wave amplitudes are found for explosions at the frequencies used by ElarmS (demonstrated by Baumgardt and Ziegler, 1988, and Baumgardt and Young, 1990). Because ElarmS uses the maximum displacement of the very first arrivals for its calculations, this effect may explain the overestimation of the explosion magnitudes. Figure 6 shows an example of

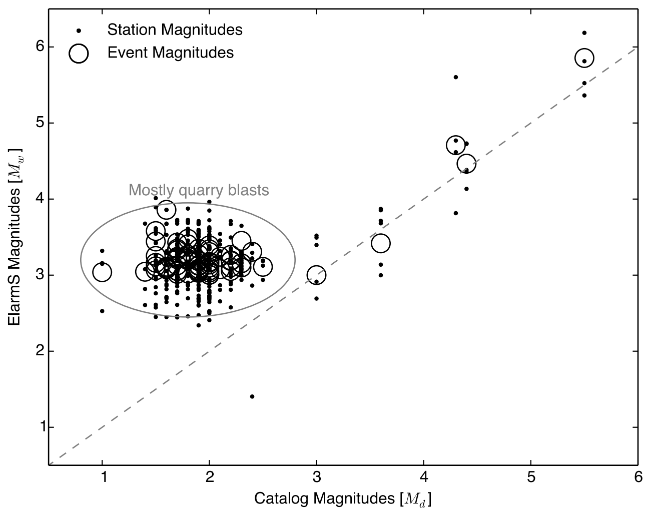

Figure 5. ElarmS real-time (RT) magnitude estimations versus GII catalog magnitudes. Event magnitudes are marked as open circles, individual station magnitudes (used for calculating the events magnitudes) are marked as dots. Note the overestimation of small ($M_D < 3$) events marked by an oval, mostly categorized as quarry blasts. The dashed line marks 1:1 relation.

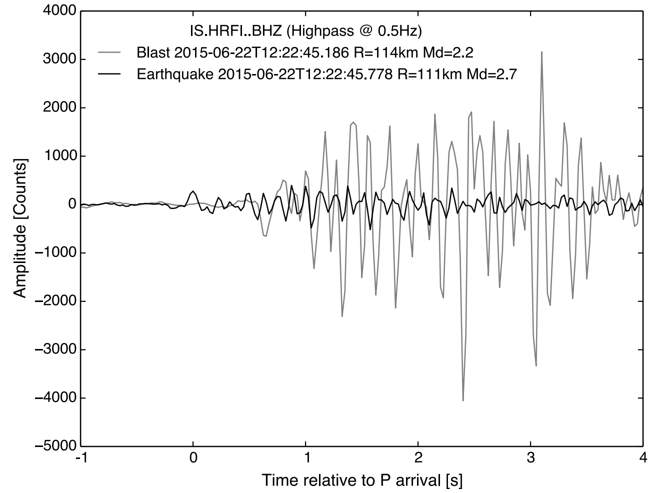

Figure 6. Traces of two events recorded by station IS.HRFI on channel BHZ at 40 samples per second. Traces are filtered using a high-pass filter at 0.5 Hz. Both events are at an ~113 km distance of the station, with a duration magnitude of M_D 2.2 (quarry blast) and M_D 2.7 (earthquake). *P* arrival is at zero time. Quarry blast (light gray) shows higher amplitudes with respect to a natural earthquake (black) for the first several seconds, potentially leading to the overestimation of the magnitude by ElarmS.

this phenomena: for two events, one categorized as a natural earthquake and one as a quarry blast, both at similar epicentral distances (~110 km) and with M_D 2.2 and 2.7 for the blast and earthquake, respectively, at ISN station HRFI. The blast waveform exhibit much higher amplitudes for the first few seconds of the trace, which leads to an overestimation of the magnitude by ElarmS. Most of the existing algorithms make use of the ratios between *P*- and *S*-wave properties to discriminate between earthquakes and quarry blasts (e.g., Kuyuk, Yildirim, *et al.*, 2014, and references therein), and are not suitable for EEW due to the delay needed for processing the *S* wave. One of our observations is that future versions of ElarmS should include a filter for quarry blasts to reduce low-magnitude false alerts of this kind.

The ElarmS algorithm requires four station triggers to issue an alert. Typically, on the GII server, the ElarmS alert is issued around 80 ms after the arrival of the last packet, which contains the fourth trigger that ultimately is needed for the declaration of an event. Alert times are in the range of 10 s to 1 min after origin time, with an average of 30 s, depending on hypocentral distances, density of stations near the event, and trigger latencies. Alert times are expected to decrease as data packet sizes and latencies are reduced in future upgrades to the ISN, and with the addition of more stations.

Real-Time Performance for two $M_w > 4.0$ Events

The 27 June 2015 M_w 5.5 Nuweiba Event. The most significant event during the analysis period was the 27 June 2015 M_w 5.5 Nuweiba event (28.877° latitude; 34.707° longitude; Fig. 7a). This earthquake was felt all across Israel, but only caused negligible damage. However, the epicenter for this event was in proximity to the 22 November 1995 M_w 7.2 Nuweiba event (Baer *et al.*, 2008, and references therein), which resulted in severe damage to the nearest (~80 km) Israeli city of Eilat. Figure 8a shows a timeline for the event. Catalog origin time for the M_w 5.5 Nuweiba event was 15:33:59.568 and the *S*-wave arrival time (representing the beginning of shaking) at Eilat (EIL station) was 15:34:27.190, 27.622 s after origin time. ElarmS successfully issued an early warning alert for this event at 15:34:26.330, 0.86 s before the arrival of the *S* wave at Eilat. The long delay in issuing the alert was due to the network geometry and large latencies of the yet-to-be optimized ISN stations. The arrival time for the *P* wave at the fourth station (HRFI, located 132 km from the epicenter) was 15:34:22.078 (22.51 s after origin time), and the waveform did not arrive at the ElarmS buffer until 15:34:26.267, which equates to an additional 4.189 s delay. The alert was issued only 63 ms later, so it is the scarcity of stations in the epicentral region and the packetization and delivery of data to the server that are responsible for the majority of the delay. Mean latency at HRFI was 2.7 s, but the packet size was 8.1 s (with the trigger 7.325 s from the start of the packet). We replayed the event in RTP mode, with an average latency of 3 s for all stations, and found that reducing packet sizes would have added ~1 s to the early warning time, and thus, issuing an alert 1.9 s before the arrival of the *S* waves to the city of Eilat. This relatively small improvement is doable due to the position of the trigger in the packet. Because the trigger occurred in the last second of the packet, the alert time was increased only by 1 s. In a scenario where the trigger occurred at the beginning of packet, the alert time would have significantly improved. Reducing latencies from 3 to 1 s would result in an alert ~3.5 s before the arrival of the *S* wave.

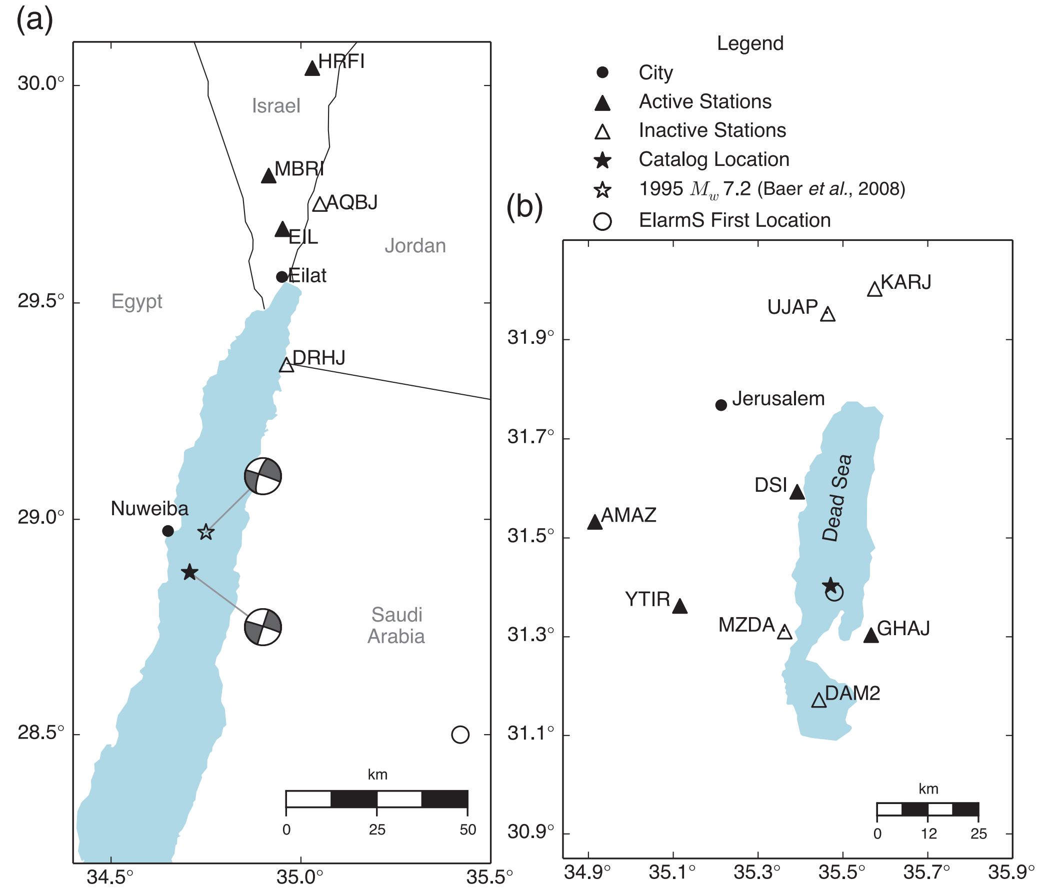

Figure 7. Location map for two RT events. (a) The 27 June 2015 M_D 5.5 Nuweiba event. (b) The 30 July 2015 M_D 4.4 Dead Sea event. Catalog location is marked as dark star. ElarmS location is marked as a circle. Active stations used for first location are marked as filled triangles. Inactive stations are marked by open triangles. The location of the 22 November 1995 M_w 7.2 Nuweiba event is marked as open star. Moment tensor solution is after Baer *et al.* (2008).

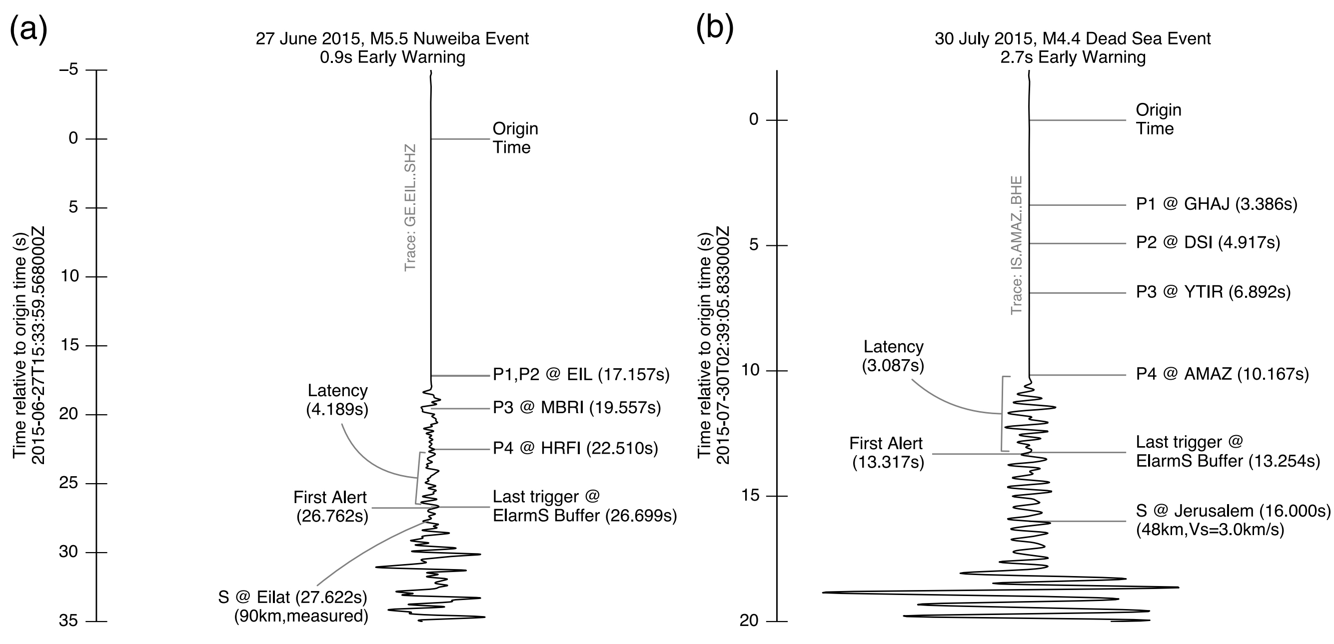

Figure 8. Timeline scheme for the RT processing of (a) the 27 June 2015 M_D 5.5 Nuweiba event and (b) the 30 July 2015 M_D 4.4 Dead Sea event. *Px*, *P*-wave arrival time at a station, in which *x* is the station trigger order of arrival. *S*, *S*-wave arrival at a location.

Table 2
List of Simulation Earthquake Parameters

Number	Origin Time (hh:mm:ss)	M_w	Latitude (°)	Longitude (°)	Moment	Strike (°)	Dip (°)	Rake (°)
1	09:05:00	5.1	31.872	35.497	4.5×10^{16}	88	72	−142
2	09:34:50	5.8	32.117	35.557	5.0×10^{17}	190	70	0
3	10:17:05	6.9	31.983	35.498	2.2×10^{19}	202	77	15
4	12:17:05	7.8	35.2	27.5	5.0×10^{20}	50	30	25

Depth fixed at 10 km.

Table 3
ElarmS Solutions for Simulated Earthquakes

Number	Origin Time (hh:mm:ss.ss)	M_w	Latitude (°)	Longitude (°)	Origin Time Error (s)	M_w Error	Local Error (km)
1	09:05:00.32	5.7	31.8801	35.4643	0.32	0.6	3.22
2	09:34:49.74	5.6	32.1099	35.6387	−0.26	−0.2	7.75
3	10:17:05.23	6.7	31.988	35.5492	0.23	−0.2	5.87
4	12:18:12.80	7.5	33.2904	33.0402	−67.8*	−0.3	686.81*

Depth fixed at 8 km.
*Error is a result of the location search grid limits (see text for more details).

This event is also a good example of the potential usefulness of adjacent seismic networks, such as the JSN in Jordan. Two of the JSN BB stations, AQBJ and DRHJ, are located at 100 and 60 km from the epicenter, but were not available for processing. If JSN data were available, alert times would have been increased to a maximum of ~10.5 s, depending on data delays.

The 30 July 2015 M_D 4.4 Dead Sea Event. An M_D 4.4 event, felt in many areas across Israel, occurred on 30 July 2015 at 02:39:05.833 (GII catalog origin time), 48 km from Jerusalem at the center of the Dead Sea (31.403° latitude; 35.471° longitude; Fig. 7b). Assuming *S*-wave velocity of 3 km/s, the *S*-wave arrival time at Jerusalem is estimated at 02:39:21.833 (16 s after the origin time). Figure 8b shows a timeline for the event. The ElarmS first alert was issued at 02:39:19.150 (13.317 s after the origin time), giving ~2.6 s of early warning for Jerusalem. The first magnitude estimation was M_w 4.47, with a location error of 1.57 km and an origin-time error of 0.68 s. The alert was issued only 63 ms after the *P* wave arrived at AMAZ; the fourth triggered station needed to issue an alert. The AMAZ packet size was 3.31 s (trigger at 2.05 s from the packet start), and the packet latency was 3.1 s, leading to a data delay of 4.36 s. Reducing the latency and packet size to 1 s could have added about 2.36 s to the early warning time, giving a total of ~5 s to Jerusalem before the onset of shaking.

Earthquake Simulations

We use a set of four large earthquake scenarios (Table 2) to test ElarmS. Seismic waveforms were simulated for ISN stations using AXITRA (Coutant, 1990). AXITRA is a numerical code that, based on the reflectivity method (Müller, 1985; Kennett, 2009), evaluates Green's functions for laterally homogeneous elastic media and approximates a full wavetrain at each station (receiver) by convolving a given source function with the computed Green's functions. Additional technical details and results of the simulation are described by Pinsky (2014). The simulated waveforms, originally provided as individual Seismic Analysis Code files for each channel, with counts representing velocity measurements, were streamed to ElarmS in ATP mode. The ElarmS results are summarized in Table 3. All four simulated events were detected and alerted upon, with no false alerts.

Magnitude errors for the simulated data are less than 0.3 magnitude units, origin-time errors are ~0.3 s and location errors are less than 10 km, except for the M_w 7.8 (event 4), originally located south of the Greek Karpathos Dodecanese Island. The poor solution of this event is due to its distance from the seismic network and the fact that ElarmS locates events on a grid limited to 200 km from the stations (Kuyuk, Allen, *et al.*, 2014). Thus, ElarmS located the event ~200 km from the triggered stations, at the edge of its search grid. Although the simulations were computed using the GII velocity model (Feigin and Shapira, 1994), the default ElarmS velocity model was used for processing, suggesting that the velocity model has little impact on the results. This first successful attempt at using ElarmS for processing synthetic data demonstrates the potential of using synthetic data for testing and evaluating the ElarmS system in different scenarios, both for the current Israeli network and for other networks.

Discussion and Conclusions

In this article, we investigate how the ElarmS EEWS performs outside of its original optimized region of California. To adapt ElarmS to the Israeli region, where seismicity rates are significantly lower and historical data are limited for moderate and strong earthquakes, we analyze (1) historical data playbacks, (2) RT processing, and (3) simulated data.

ElarmS has now been modified to be compatible with the network geometry in and around Israel. We find that it is necessary to use a regionally developed magnitude estimation equation to relate maximum displacement P_d with magnitude. The magnitude relation previously derived from an independent dataset (Sadeh *et al.*, 2014) is an excellent fit between catalog magnitudes and ElarmS results for historical data with $3 < M_D \leq 5.3$ and for several available RT $M_D > 3$ events. We note that data used here do not include large magnitude earthquakes and therefore using the adjusted magnitude relations should be done with care.

We are satisfied that RT results exhibit good performance. Only two false alerts were reported (M_w 3.4 and 3.2) and no earthquakes of $M_D > 3$ were missed. However, the alert times are currently very short as the ISN is not optimized for RT warnings and suffers from large latencies and long data packets. ElarmS does detect the large number of explosive sources in the region and tends to overestimate their magnitude due to higher amplitude P waves from these sources. However, events with the overestimate of magnitude are all $M_w < 3.5$ so applying a minimum magnitude threshold of M_w 3.5 to issue an alert resolves this issue. The development of additional filters to differentiate between blasts and natural earthquakes is underway and will be implemented in the future versions of ElarmS.

For the first time, we test the use of synthetic data to evaluate ElarmS performance. The results are encouraging because they show that events located less than 200 km from the network edge were located in a range of less than 10 km from the epicenter and ~0.3 of origin time. Magnitude estimations were in the range of 0.3 magnitude units. For future planning, scenario-based testing will be needed. Further work is also required to generate more complete synthetic data incorporating 3D velocity models, noise, latencies, various rupture lengths and geometries, simultaneous events, preshocks or aftershocks, etc.

The methods and tools described in this work may be useful for implementing ElarmS in other regions, and similar efforts are being made in the US Pacific Northwest, Chile, Turkey, and South Korea. ElarmS has the potential to aid populations at risk to receive an early warning of seconds to tens of seconds to minutes before the arrival of destructive waves. The algorithm simplicity as well as the robustness and speed are highly suited to regions with limited seismic data availability. Nevertheless, efforts will be needed to verify and adjust ElarmS in any new region.

Data and Resources

Seismograms used in this study were collected by the Geophysical Institute of Israel (GII). Data can be obtained from GII at http://www.gii.co.il/ (last accessed August 2015). Moment tensor solution in Figure 7 acquired from U.S. Geological Survey at http://earthquake.usgs.gov/ (last accessed November 2015). Figures in this article were produced by Python 2D plotting module Matplotlib (Hunter, 2007) and ObsPy (Beyreuther *et al.*, 2010). The tools created and used for analysis of data in this article are available at https://github.com/rannof (last accessed December 2015). Map used in the graphical user interface (GUI) tools is available at http://www.openstreetmap.org/ (last accessed December 2015)

Acknowledgments

The Geological Survey of Israel (GSI), at the Ministry of Energy and Water Resources, funded this research. The authors would like to thank the Geophysical Institute of Israel (GII) technical and research team for their cooperation and help with historical and simulated data.

References

Allen, R. M., G. Baer, J. Clinton, Y. Hamiel, R. Hofstetter, V. Pinsky, A. Ziv, and A. Zollo (2012). Earthquake early warning for Israel: Recommended implementation strategy, *Report GSI/26/2012*, Geological Survey of Israel, Jerusalem, Israel.

Allen, R. M., H. Brown, M. Hellweg, O. Khainovski, P. Lombard, and D. Neuhauser (2009). Real-time earthquake detection and hazard assessment by ElarmS across California, *Geophys. Res. Lett.* **36,** no. 5, L00B08, doi: 10.1029/2008GL036766.

Allen, R. M., M. Hellweg, D. Neuhauser, I. Henson, and J. Strauss (2015). CISN earthquake early warning 2014, *13th Annual Northern California Earthquake Hazards Workshop*, Menlo Park, California, 26–27 January 2016.

Ambraseys, N. N., J. Douglas, S. K. Sarma, and P. M. Smit (2005). Equations for the estimation of strong ground motions from shallow crustal earthquakes using data from Europe and the Middle East: Horizontal peak ground acceleration and spectral acceleration, *Bull. Earthq. Eng.* **3,** no. 1, 1–53, doi: 10.1007/s10518-005-0183-0.

Avni, R., D. Bowman, A. Shapira, and A. Nur (2002). Erroneous interpretation of historical documents related to the epicenter of the 1927 Jericho earthquake in the Holy Land, *J. Seismol.* **6,** no. 4, 469–476, doi: 10.1023/A:1021191824396.

Baer, G., G. J. Funning, G. Shamir, and T. J. Wright (2008). The 1995 November 22, M_w 7.2 Gulf of Elat earthquake cycle revisited, *Geophys. J. Int.* **175,** no. 3, 1040–1054, doi: 10.1111/j.1365-246X.2008.03901.x.

Baumgardt, D. R., and G. B. Young (1990). Regional seismic waveform discriminants and case-based event identification using regional arrays, *Bull. Seismol. Soc. Am.* **80,** no. 6, 1874–1892.

Baumgardt, D. R., and K. A. Ziegler (1988). Spectral evidence for source multiplicity in explosions: Application to regional discrimination of earthquakes and explosions, *Bull. Seismol. Soc. Am.* **78,** no. 5, 1773–1795.

Beyreuther, M., R. Barsch, L. Krischer, T. Megies, Y. Behr, and J. Wassermann (2010). ObsPy: A Python toolbox for seismology, *Seismol. Res. Lett.* **81,** no. 3, 530–533, doi: 10.1785/gssrl.81.3.530.

Böse, M., R. Allen, H. Brown, G. Gua, M. Fischer, E. Hauksson, T. Heaten, M. Hellweg, M. Liukis, D. Neuhauser, *et al.* (2014). CISN ShakeAlert: An earthquake early warning demonstration system for California, in *Early Warning for Geological Disasters*, F. Wenzel and J. Zschau (Editors), Springer, Berlin, Heidelberg, 49–69.

Böse, M., E. Hauksson, K. Solanki, H. Kanamori, and T. H. Heaton (2009). Real-time testing of the on-site warning algorithm in southern California and its performance during the July 29 2008 M_w 5.4 Chino Hills earthquake, *Geophys. Res. Lett.* **36,** no. 3, L00B03, doi: 10.1029/2008GL036366.

Campbell, K. W., and Y. Bozorgnia (2006). Next generation attenuation (NGA) empirical ground motion models: Can they be used in Europe?, *First European Conference on Earthquake Engineering and Seismology*, Geneva, Switzerland, 10 pp.

Coutant, O. (1990). Programme de Simulation Numerique AXITRA, *Rapport LGIT*, Université Joseph Fourier, Grenoble, France.

Cua, G., M. Fischer, T. Heaton, and S. Wiemer (2009). Real-time performance of the virtual seismologist earthquake early warning algorithm in southern California, *Seismol. Res. Lett.* **80,** no. 5, 740–747, doi: 10.1785/gssrl.80.5.740.

Erdik, M., Y. Fahjan, O. Ozel, H. Alcik, A. Mert, and M. Gul (2003). Istanbul earthquake rapid response and the early warning system, *Bull. Earthq. Eng.* **1,** no. 1, 157–163, doi: 10.1023/A:1024813612271.

Espinosa-Aranda, J. M., A. Cuéllar, F. H. Rodríguez, B. Frontana, G. Ibarrola, R. Islas, and A. García (2011). The seismic alert system of Mexico (SASMEX): Progress and its current applications, *Soil Dynam. Earthq. Eng.* **31,** no. 2, 154–162, doi: 10.1016/j.soildyn.2010.09.011.

Feigin, G., and A. Shapira (1994). A unified crustal model for calculating travel times of seismic waves across the Israel seismic network, *Report Z1/567/79(107)*, Geophysical Institute of Israel, Lod, Israel.

Garfunkel, Z., I. Zak, and R. Freund (1981). Active faulting in the dead sea rift, *Tectonophysics* **80,** no. 1–4, 1–26, doi: 10.1016/0040-1951(81)90139-6.

Hamiel, Y., R. Amit, Z. B. Begin, S. Marco, O. Katz, A. Salamon, E. Zilberman, and N. Porat (2009). The seismicity along the Dead Sea Fault during the Last 60,000 Years, *Bull. Seismol. Soc. Am.* **99,** no. 3, 2020–2026, doi: 10.1785/0120080218.

Hsiao, N.-C., Y.-M. Wu, T.-C. Shin, L. Zhao, and T.-L. Teng (2009). Development of earthquake early warning system in Taiwan, *Geophys. Res. Lett.* **36,** no. 2, L00B02, doi: 10.1029/2008GL036596.

Hunter, J. D. (2007). Matplotlib: A 2D graphics environment, *Comput. Sci. Eng.* **9,** no. 3, 90–95, doi: 10.1109/MCSE.2007.55.

Ionescu, C., M. Böse, F. Wenzel, A. Marmureanu, A. Grigore, and G. Marmureanu (2007). An early warning system for deep Vrancea (Romania) earthquakes, in *Earthquake Early Warning Systems*, P. Gasparini, G. Manfredi, and J. Zschau (Editors), Springer, Berlin and Heidelberg, Germany, 343–349.

Kennett, B. L. N. (2009). *Seismic Wave Propagation in Stratified Media*, ANU E Press, Acton, Canberra, ACT.

Kuyuk, S. H., and R. M. Allen (2013a). A global approach to provide magnitude estimates for earthquake early warning alerts, *Geophys. Res. Lett.* **40,** no. 24, 6329–6333, doi: 10.1002/2013GL058580.

Kuyuk, S. H., and R. M. Allen (2013b). Optimal seismic network density for earthquake early warning: A case study from California, *Seismol. Res. Lett.* **84,** no. 6, 946–954, doi: 10.1785/0220130043.

Kuyuk, S. H., R. M. Allen, H. Brown, M. Hellweg, I. Henson, and D. Neuhauser (2014). Designing a network-based earthquake early warning algorithm for California: ElarmS-2, *Bull. Seismol. Soc. Am.* **104,** no. 1, 162–173, doi: 10.1785/0120130146.

Kuyuk, S. H., E. Yildirim, E. Dogan, and G. Horasan (2014). Clustering seismic activities using linear and nonlinear discriminant analysis, *J. Earth Sci.* **25,** no. 1, 140–145, doi: 10.1007/s12583-014-0406-x.

Levi, T., B. Tavron, O. Katz, R. Amit, D. Segal, Y. Hamiel, Y. Bar-Lavi, S. Romach, and A. Salamon (2010). Earthquake loss estimation in Israel using the new HAZUS-MH software: Preliminary implementation, *Report GSI/11/2010*, Geological Survey of Israel, Jerusalem, Israel.

Müller, G. (1985). The reflectivity method: A tutorial, *J. Geophys.* **58,** 153–174.

Nakamura, Y. (1988). On the urgent detection and alarm system (UrEDAS), *Ninth World Conference on Earthquake Engineering*, 673–678.

Nakamura, Y., and J. Saita (2007). UrEDAS, the earthquake warning system: Today and tomorrow, in *Earthquake Early Warning Systems*, P. Gasparini, G. Manfredi, and J. Zschau (Editors), Springer, Berlin and Heidelberg, Germany, 249–282.

Pinsky, V. (2014). Building a tool for seismological exercise of processing large earthquakes at ISN, *Report 030/785/14*, Geophysical Institute of Israel, Lod, Israel.

Pinsky, V. (2015). Modeling warning times for the Israel's earthquake early warning system, *J. Seismol.* **19,** no. 1, 121–139, doi: 10.1007/s10950-014-9454-z.

Sadeh, M., A. Ziv, and H. Wust-Bloch (2014). Real-time magnitude proxies for earthquake early warning in Israel, *Geophys. J. Int.* **196,** no. 2, 939–950, doi: 10.1093/gji/ggt407.

Satriano, C., L. Elia, C. Martino, M. Lancieri, A. Zollo, and G. Iannaccone (2011). PRESTo, the earthquake early warning system for Southern Italy: Concepts, capabilities and future perspectives, *Soil Dynam. Earthq. Eng.* **31,** no. 2, 137–153, doi: 10.1016/j.soildyn.2010.06.008.

Shapira, A. (1988). Magnitude scales for regional earthquakes monitored in Israel, *Isr. J. Earth Sci.* **37,** no. 1, 17–22.

Shapira, A., and R. Hofstetter (2007). Earthquake hazard assessments for building codes, *Final report*, Geophysical Institute of Israel, Lod, Israel.

Shapira, A., R. Avni, and A. Nur (1993). A new estimate for the epicenter of the Jericho earthquake of 11 July 1927, *Isr. J. Earth Sci.* **42,** 93–96.

Sheen, D.-H., I.-S. Lim, J.-H. Park, and H.-C. Chi (2014). Magnitude scaling relationships using *P* waves for earthquake early warning in South Korea, *Geosci. J.* **18,** no. 1, 7–12, doi: 10.1007/s12303-013-0066-3.

Worden, C. B., M. C. Gerstenberger, D. A. Rhoades, and D. J. Wald (2012). Probabilistic relationships between ground-motion parameters and modified Mercalli intensity in California, *Bull. Seismol. Soc. Am.* **102,** no. 1, 204–221, doi: 10.1785/0120110156.

Yucemen, M. S. (1992). Seismic hazard maps for Jordan and vicinity, *Nat. Hazards* **6,** no. 3, 201–226, doi: 10.1007/BF00129509.

Appendix

A set of tools were created to allow rapid deployment and analysis of the ElarmS system. These tools were developed using a combination of the Python scripting language and C programming language, combining the ease and rapid development of Python with the robustness and fast performance of C.

The main objectives of the tools were to (a) allow a real-time (RT) visual monitoring of ElarmS system modules and components, (b) enable RT and accelerated-time playbacks of historical data, and (c) review the log files and investigate ElarmS performance with respect to the Israeli Seismic Network (ISN) offline catalog.

The tools are now available online (see Data and Resources). A brief description can be found below.

ElViS

Elarms Visualization System (ElViS) is a graphical user interface (GUI) tool. It is connected to the ElarmS messaging system (ActiveMQ) and receives messages from the various modules and displays their content in a simple graphical way (Fig. A1). The tool follows ShakeAlert's USERDISPLAY calculation methods, but is aimed at system administrators rather than end users. The tool is based on the Python module Matplotlib (Hunter, 2007). The current version has the following features:

- display of user predefined location (can be changed interactively);
- display of active/inactive stations locations and their current maximal acceleration/velocity/displacement;
- display of the trigger message logs from the EWP2 module;

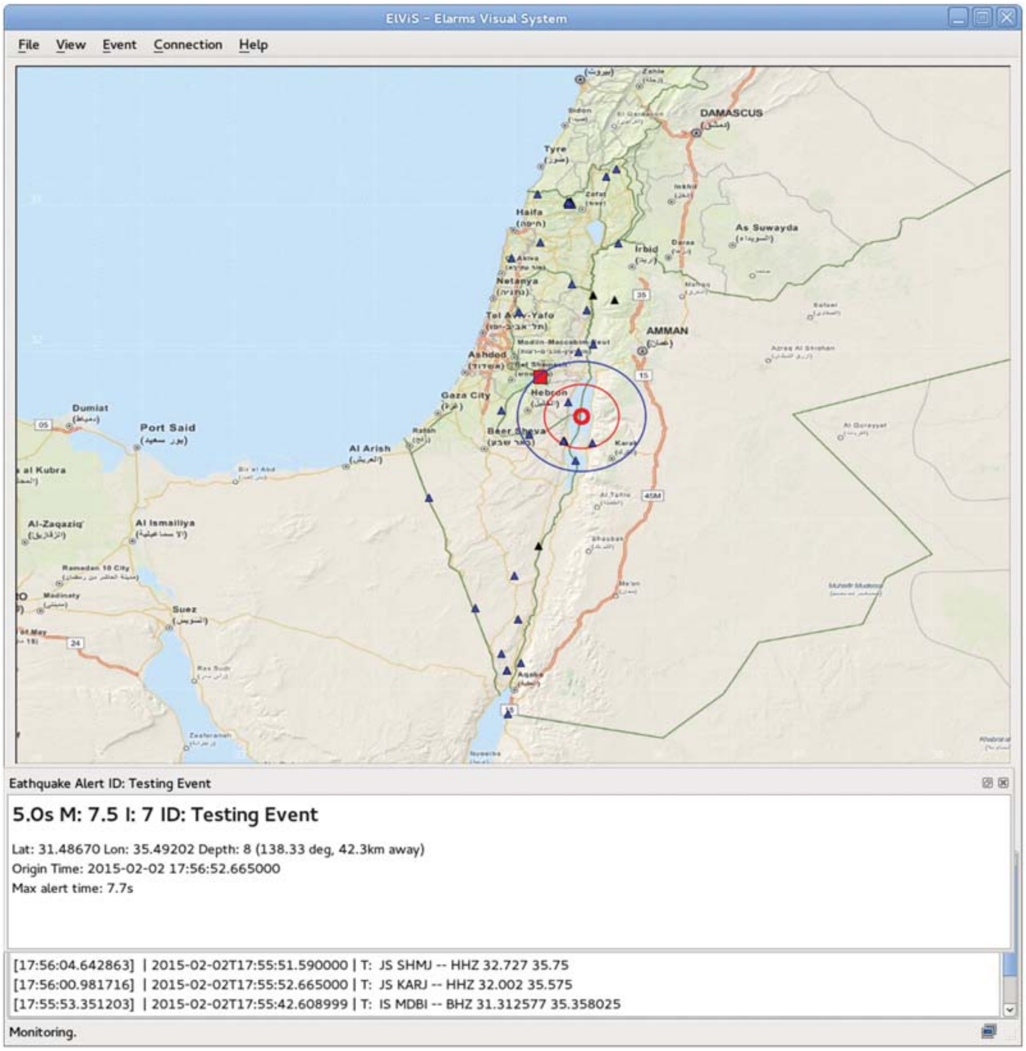

Figure A1. ElarmS Visualization System (ElViS) screenshot. Colors of stations (triangles) indicate acceleration envelope values (colors) or station inactivity (i.e., no data, black). The red square represents point of reference for calculating *S*-wave arrival time and expected intensity. Background maps are rendered online from open street maps (see Data and Resources). This example shows an event alert test. Upon receiving an alert, the event location is marked as a bold red circle, *P*- and *S*-wave real-time propagation is marked as blue and red circles, respectively, and event information is given on a panel below the map, stating estimated moment magnitude (M_w 7.5), expected arrival time of *S* wave (5.0 s) and intensity (*I* 7) with respect to the user location (red square). The information also includes the event location as latitude, longitude, depth, azimuth, and distance from the reference point, the origin time of the event and the maximum alert time (the first *S*-wave arrival-time estimation, 7.7 s in this case).

- display of event message logs from the E2 module and decision module (DM);
- display an indication ActiveMQ connection;
- display event location and parameters;
- interactively send an event message to the ActiveMQ upon receiving an event alert from the E2 module or DM (can also simulate an alert of user-defined parameters);
- calculate and display the remaining warning time for the user location based on a simple distance to epicenter and a constant wave velocity;
- calculate and display the expected modified Mercalli intensity (Worden *et al.*, 2012, their equation 3) at the user-defined location;
- display of ElarmS estimated magnitude; and
- calculate and display *P*- and *S*-wavefronts (based on a constant wave velocity).

SRTPB

SeedLink Real-Time Playback (SRTPB) is capable of reading waveform data from files supported by the Python module ObsPy (Beyreuther *et al.*, 2010) and sending them to a SeedLink server, or saving them into a file. The data are repacked in packets of specified time intervals (typically 1 s) and ordered according to packet start time. Packets are then either sent in RT speed, or accelerated speed allowing a playback of historic, or simulated data. In addition, the tool can

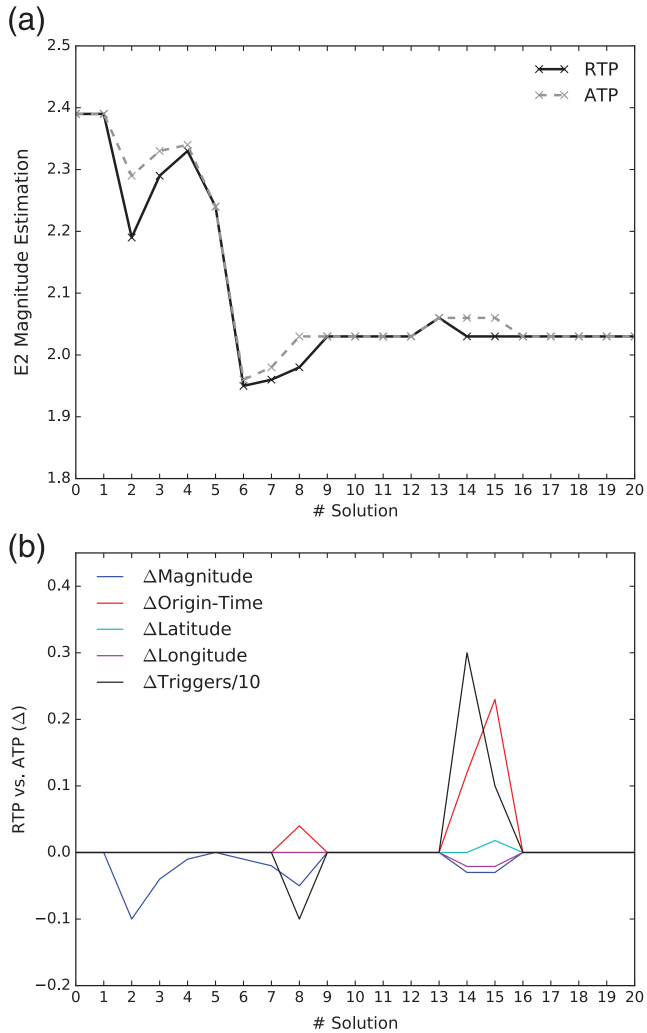

Figure A2. A comparison of real-time playback (RTP) and accelerated-time playback (ATP) results using the SeedLink Real-Time Playback (SRTPB) tool for 21 January 2015, M_D 2.4 event selected randomly. (a) Magnitude estimation at each successive solution of the E2 module. RTP is marked by the solid line and ATP by the dashed line. ATP is set with a 0.1 s interval every 250 packets sent to the SeedLink server buffer to avoid overload of ElarmS buffers. (b) Difference in source parameters solutions between the RTP and ATP. Differences are very small but not exactly the same due to the unrepeatable nature of ElarmS multiprocessing modules.

manipulate the data packet's original time to account for predefined station latencies or to adjust time to the current time. The latter is most useful in conjunction with ElViS or USERDISPLAY for evaluating alert times in a realistic scenario. For accelerated performance, data packets can be repacked and reordered and saved into a file to be sent directly to a SeedLink server at a later stage. This method allows replaying the same data multiple times more efficiently. Figure A2 shows a comparison of real-time playback (RTP) and accelerated-time playback (ATP) results. The differences are very small but not exactly the same due to the unrepeatable nature of ElarmS multiprocessing modules.

E2log2SC

E2log2SC converts E2 log files to Seiscomp3 event parameters xml files. This tool enables the analysis of the ElarmS results using the Seiscomp3 tools and importing the results to a Seiscomp3 database.

E2ReviewTool

E2ReviewTool is a GUI tool designed to read ElarmS log files and present the data as maps and tables, thus allowing analysis of the system performance. The current version has the following features:

- read ElarmS E2 module log files and a catalog list of events;
- associate ElarmS events and catalog events based on origin time and location;
- present an interactive map of catalog events and ElarmS events, with a color scheme for matched, missed, and false events (station locations are also available on the map);
- a table of all event information (origin time, location, magnitude, errors);
- a summary of performance (number of matched, missed, and false alerts);
- plots and histograms of magnitude estimation quality, compared with the catalog;
- a list of ElarmS solution evolution with time for each event;
- a list of ElarmS triggers used to solve each event, their properties, and relevant information; and
- filters events for certain magnitude, time, and space windows.

Berkeley Seismological Laboratory
University of California, Berkeley
Berkeley, California 94703
ran.nof@gmail.com

Manuscript received 13 January 2016;
Published Online 23 August 2016